

Spider monkey optimization (SMO) – lattice Levenberg–Marquardt recursive least squares based grid synchronization control scheme for a three-phase PV system

Dipak Kumar DASH, Pradip Kumar SADHU and Bidyadhar SUBUDHI

This paper presents a new grid integration control scheme that employs spider monkey optimization technique for maximum power point tracking and Lattice Levenberg Marquardt Recursive estimation with a hysteresis current controller for controlling voltage source inverter. This control scheme is applied to a PV system integrated to a three phase grid to achieve effective grid synchronization. To verify the efficacy of the proposed control scheme, simulations were performed. From the simulation results it is observed that the proposed controller provides excellent control performance such as reducing THD of the grid current to 1.75%.

Key words: solar PV array, VSC, SMO, DC-DC converter, lattice Levenberg–Marquardt recursive least squares; hysteresis current controller

1. Introduction

Photovoltaic power generation is considered as one of the most efficient renewable options for supplementing conventional power owing to several advantages such as abundant solar irradiance and pollution free power. There are a number of issues involved in integrating a PV system into a grid. The PV panel output characteristics are affected by the external factors namely temperature, solar irradiance [1]. In energy generation of PV systems, the maximum power extraction technique is a major concern for improving the effectiveness where there is non-uniform solar irradiance and shading [3]. Perturb and observe (P&O), fuzzy logic

Copyright © 2021. The Author(s). This is an open-access article distributed under the terms of the Creative Commons Attribution-NonCommercial-NoDerivatives License (CC BY-NC-ND 4.0 <https://creativecommons.org/licenses/by-nc-nd/4.0/>), which permits use, distribution, and reproduction in any medium, provided that the article is properly cited, the use is non-commercial, and no modifications or adaptations are made

D.K. Dash (e-mail: dipak.nitrkl@gmail.com) and P.K. Sadhu (e-mail: pradip@iitism.ac.in) are with Department of Electrical Engineering, Indian Institute of Technology (ISM), Dhanbad, India.

B. Subudhi (corresponding author, e-mail: bidyadhar@iitgoa.ac.in) is with School of Electrical Sciences, Indian Institute of Technology Goa, GEC Campus, Farmagudi, Ponda-401403, Goa, India.

Received 09.01.2021. Revised 19.05.2021.

control and Incremental Conductance, etc., are the most generally used maximum power point tracking algorithms in small and large size of PV applications [4]. Efficient control techniques need to be designed for the optimal operation of switching converter and employed for PV system integrated to grid [8]. The generated power from the PV system is supplied to the neighboring loads, subsequent to fulfilling the load demand then the remaining power is provided to the grid [6]. Yet, if the load demand is not fulfilled by the generated solar power then the power demand is met by the grid [10]. The high diffusion of PV in grid can cause the voltage instability problem. Also, it impacts the phase imbalance and frequency of the grid coordinated system. Consequently, the power quality issues arise in the load side as well as grid side at the time of grid connected to the distributed system [11]. It is a challenge in the grid connection for maintaining the synchronization, steadiness, reliability and behavior of the whole system [7]. Therefore, it is necessary to design efficient control mechanism to control the power quality problems arising in a Solar PV system [13]. Generally, various types of control algorithms have been proposed for a grid connected PV system such as symmetrical component theory, Least Mean Square [14], Sliding Mode Control [23], and Instantaneous Reactive Power Theory [24]. However, opportunity lies to further improve the controller design for improving the grid behavior and reliability [15]. Hence, the objective of this work is to develop a new control algorithm with an efficient MPPT for enhancing the performance of grid coordinated system from the quality problems.

In this paper, the SPV array has been coupled to the grid with three phase VSC, the control algorithm based on LLMRLS method has been implemented for control of reference grid currents generation and gating pulses for the 3φ VSC. Consequently, the behavior of the advanced control design has demonstrated and the satisfactory operation of load power demand is attained along with the power quality issues such as the UPF maintaining, harmonic removal and load unbalancing. Grid current is achieved at 1.75% of THD in the PF correction and the PCC voltage along with the Load current THDs also satisfied within the limit of IEEE 519 standard.

This paper is organized as follows. In section 2, different methods to mitigate power quality issues has been discussed. The proposed control scheme with control strategy is presented in section 3. In section 4 numeric simulation results are presented and discussed. Finally, conclusions are discussed in section 5.

2. Related work

Some of the recent literature [5] whilst resolving power quality issues, proposed the solution to PQ problems and improving the grid coherent solar PV system behavior. Integration of renewable energy system to grid affects solar

irradiance and shading on panels. PQ problems caused by the nonlinear loads. To resolve this issue, Subarni et al. proposed Decorrelation Normalized Least Mean Square (DNLMS) algorithm based grid synchronizing control scheme [16]. The P&O MPPT algorithm was extensively used for maximum solar power extraction. The Power Quality problems arise because of the nonlinear loads originating worsen power factor (PF) and voltage regulation crisis in AC grid. Vandana et al. proposed the Hyperbolic Tangent Function (HTF) with higher order adaptive control algorithm among the P&O based MPPT algorithm for a grid synchronization of PV system [17].

A two-stage topology of grid-integrated PV system is employed with the nonlinear, which is encountered with PQ problems. Nishant et al. proposed the learning based incremental conductance of MPPT algorithm in addition to the leaky least logarithmic absolute difference based control algorithm for the grid-connected PV system which is implemented at the Point of Common Coupling (PCC) connection [18].

In the distribution system, the PQ problems in the grid are a major problem due to the nonlinear loads. Therefore, Priyank et al. [19] proposed the Improved Second-Order Generalized Integrator with Frequency Locked Loop (ISOGI-FLL) based control design for grid-coupled Solar PV array with a VSC to mitigate the PQ problems and the steepest descent MPPT technique has been employed for the extraction of maximum power from PV array and it has maintained the DC link voltage to the desired value effectively [27]. Power quality problems arise in VSC such as harmonics and voltage fluctuations. Vandana et al. proposed the Multiple-Improved-Notch Filter based Quadrature Signal Generator (MINF- QSG) along with P&O based MPPT algorithm for a three phase single stage grid connected PV system [20, 30]. Ryszard Gessing proposed a simple proportional controller with state feedback technique for accounting the minimum and nonminimum phase of DC-DC boost converter [31]. A. Talha et al. discussed Perturb and observe and incremental inductance controllers can be improved using fuzzy logic controllers [32]. S.N. Singh et al. proposed a DPWM strategy to minimize the THD [33]. The behavior of the grid power quality is enhanced when this method is applied under the load unbalancing.

In this investigation, the Lattice Levenberg–Marquardt Recursive Least Squares (LLMRLS) control algorithm that calculates elementary weights extraction of active and reactive load currents is proposed. DC link voltage is integrated to the grid interfaced inverter which is stabilized by the DC link capacitors. The gate signal controlled algorithm is controlled by applying the HC controller. Based on this proposed technique, the grid integrated PV system performance behavior improved under balancing and unbalancing nonlinear loads. Furthermore, the varied Solar Insolation is considered.

3. Proposed control scheme

A double stage PV-Voltage source converter based system is connected with a three phase (3ϕ) grid is shown in Fig. 1. This grid connected solar PV system comprises of 3ϕ grid, PV array, VSC, nonlinear loads, ripple filter, boost converter and interfacing inductors. From this PV power generation system, the maximum power delivered from PV array is tracked by applying the Spider Monkey Optimization based MPPT algorithm. Furthermore, in VSC, switching ripple the higher order harmonics are produced, which is reduced by the ripple filter. Moreover, the PV system is connected with VSC, therefore the current harmonics are produced which is reduced by the interfacing inductor. In addition, the reference DC link voltage is generated for maximizing the output power control.

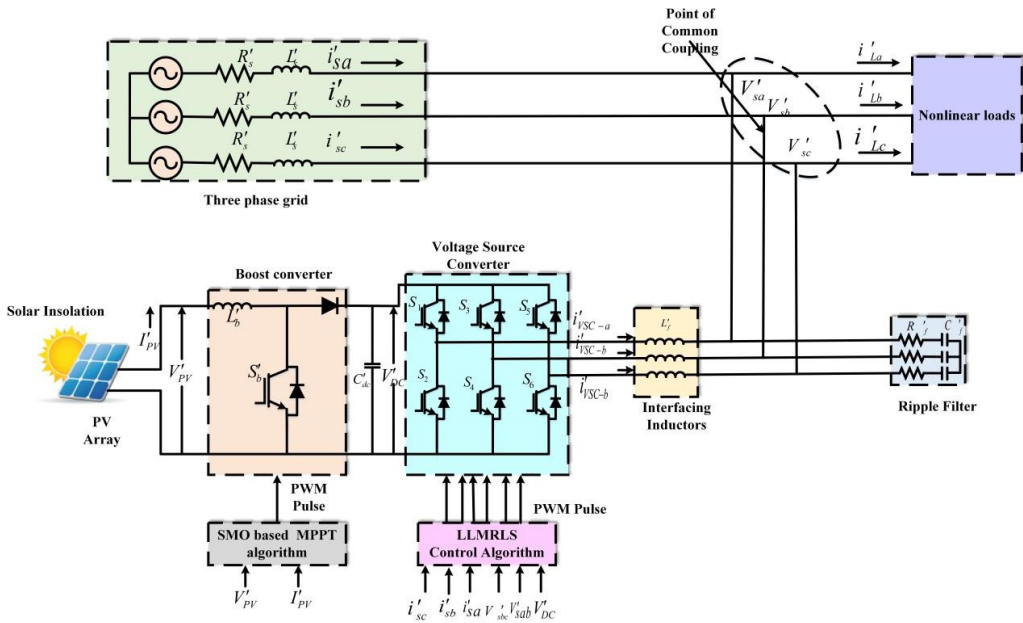


Figure 1: Schematic diagram of the proposed system

3.1. Design of solar PV array

The changing of solar energy is done via photovoltaic panel. The PV cell depends on the temperature and solar irradiance. The PV panel comprises of many solar cells connected in series and parallel. The current and voltage characteristics of a PV cell can be expressed by

$$I'_{Pv} = I'_T - I'_D, \tag{1}$$

$$I'_{Pv} = I'_T - I'_O \left[\exp \left(\frac{q (V'_{Pv} + I' R')}{\beta_a K' T_c} - 1 \right) \right], \quad (2)$$

where I'_T is the current in Ampere (A), I'_D is the diode of current (A), I'_O is the reference current (A), I'_{Pv} is the Solar PV cell current (A), q is the electronic charge (1.6×10^{-9} C), V'_{Pv} is the voltage of PV cell (V), R' is the resistance (Ω), β_a is the diode ideality factor, K' is the Boltzmann constant at (1.38×10^{-23}) and T_c is the temperature of cell in $^\circ\text{C}$ in Eq. (2). The output power from a solar PV panel is evaluated by,

$$P'_{PV} = \left(N_{PV} \times \frac{R_{ST}}{1000} \times P_{\max PV} \right) / 1000, \quad (3)$$

where the output power P'_{PV} of 11 kW, $P_{\max PV}$ is the maximum power (W/m^2), R_{ST} is the series resistance (Ω) and N_{PV} is the number of solar modules. The design of solar modules contains 96 cells in the series assortment. The voltage of open circuit each cell value is 0.28 V and the current of short circuit is 5 A is taken in simulation. The PV array can be delivered 10 kW at $1000 \text{ W}/\text{m}^2$ of solar radiation.

3.2. Spider Monkey Optimization (SMO) of MPPT algorithm

Spider Monkey Optimization (SMO) is a subclass of swarm intelligence optimization technique [26]. SMO is a food foraging based algorithm, considering nature and social frame work of spider monkeys. Fission-Fusion social system relates to social configuration of spider monkey [25]. Here, a populous, consistently dictated by a female, is fragmentized into tiny clusters for seeking, chiefly food and they are buddy up to 40/50 singular who divides into small groups in search of food who again are headed by a female [27]. In case she fails to meet the demand, then it further subdivides, again succeeded by a female, replicating the process until food is reached. The food for the spider monkey is explored in diverse directions with the help of set members, which is guided by the female aged monkey called as Global Leader (GL) [28]. Moreover, it constructs a boundary region for keeping their foods from other animals. Furthermore, if the gathered food quantity is insufficient or else if the food is insufficient in that province, the GL divides its set and initiates them to look food in various directions. At the time of food exploration, the large set is split in to the small sets. Moreover, in every set the best one is called as Local Leader (LL).

• **Initialization of population**

Primarily, n number of Sliding Modes (SM) are generated in SMO as shared primary population. The initialization of each SM_{j^*} is given by,

$$SM_{i^*j^*} = SM_{\min j^*} + \tilde{U}(0, 1) \times (SM_{\max j^*} - SM_{\min j^*}), \quad (4)$$

where $SM_{i^*j^*} = (0, 1, 2, \dots, n)$ denoted as the i^* -th SM in the population d -aspects vector, $SM_{\min j^*}$ and $SM_{\max j^*}$ are the limits of SM_{j^*} in the j^* direction and $\tilde{U}(0, 1)$ the equally shared arbitrary number in the sort $[0, 1]$.

• **LL stage**

In this stage, the SM change its location based on the statistics from the LL. The value of fitness is attained and then the new position is evaluated. The perturbation rate ($p\gamma'$) is evaluate as,

$$p\gamma_{\text{iter}^*+1} = p\gamma_{\text{iter}^*} + \left(\frac{0.4}{TnI^*} \right), \quad (5)$$

where, $p\gamma_{\text{iter}^*}$ is the current iteration value of $p\gamma$ and TnI^* is the total number of iterations articulated in Eq. (5). If the latest location value of fitness is superior to the previous location, then the SM renews its location with the new one. The SM new is expressed by the Eq. (6) as follows,

$$SM_{\text{new } i^*j^*} = SM_{i^*j^*} + \tilde{U}(0, 1) \times (L\ddot{L}_{k^*j^*} - SM_{i^*j^*}) + \tilde{U}(-1, 1) \times (SM_{r^*j^*} - SM_{i^*j^*}), \quad (6)$$

where, $SM_{i^*j^*}$ is the j^* -th aspect of the i^* -th SM, $L\ddot{L}_{k^*j^*}$ is the j^* -th aspect of the k^* -th local set leader location, $SM_{i^*j^*}$ is the j^* -th aspects of the k^* -th SM which is selected arbitrarily in k^* -th set such that $\gamma^* \neq i^*$ and $\tilde{U}(0, 1)$ is the equally shared arbitrary number in the sort $[0, 1]$ in Eq. (6).

• **GL stage**

Here all the spider monkeys renew their locations by the guidelines of GL and the member of local set. The renew location for this stage expressed in the Eq. (7) as,

$$SM_{\text{new } i^*j^*} = SM_{i^*j^*} + \tilde{U}(0, 1) \times (G\ddot{L}_{k^*j^*} - SM_{i^*j^*}) + \tilde{U}(-1, 1) \times (SM_{r^*j^*} - SM_{i^*j^*}), \quad (7)$$

where, $G\ddot{L}_{j^*}$ is the j^* -th aspects of the GL location and $j^* \in \{1, 2, \dots, d\}$ is arbitrarily selected directory. Depends upon the few probabilities the locations are renewed

by the Eq. (8) as

$$p\gamma b_{i^*} = 0.9 \times \frac{\text{fitness}_{i^*}}{\max_fitness} + 0.1, \quad (8)$$

where, fitness_{i^*} is the i^* -th SM value of fitness.

Furthermore, the newly renewed location of the SM's fitness is evaluated; it is contrasted with the previous value and takes the best one.

• **LL decision stage**

If the pre-defined threshold value is not renewed by any LL location (which is referred as LL limit), then after the locations of all set members are renewed arbitrarily initializing or by the GL or LL information combined through $p\gamma'$,

$$SM_{\text{new } i^* j^*} = SM_{i^* j^*} + \tilde{U}(0, 1) \times (G\ddot{L}_{k^* j^*} - SM_{i^* j^*}) \\ + \tilde{U}(0, 1) \times (SM_{i^* j^*} - L\ddot{L}_{k^* j^*}). \quad (9)$$

Eq. (9) shows the renewed aspects of the SM, it is fascinated on the way to the GL and keeps away from the LL. The fitness of SM is calculated.

• **Global Leader (GL) decision stage**

At the last stage, monitoring the location of the GL. moreover if the GL is not exceeded the predestined threshold, then the set is divided into fewer sets. Initially the population is divided into 2 or 3 sets furthermore, it divides till the maximum number of sets established. In addition, the position of the GL is not renewed then the GL integrates all the sets to form a one set.

In this work SMO has been characterized with the converter duty cycle (d) on the further region of PV system output power is accepted as a function of fitness. The d placed on fixed location of limits such as $SM_{\min j^*}$ and $SM_{\max j^*}$ where $SM_{\max j^*}$ is denoted as $V'_{PV_{\max}}$ and $SM_{\min j^*}$ is denoted as $V'_{PV_{\min}}$. The V'_{PV} is determined for the output power of PV system under partial weather state. Hence the V'_{PV} can be observed as the optimization variable. If an V'_{PV} is evaluated, then the d will be attained and go through the Insulated Gate Bipolar Transistor (IGBT) of VSC for the voltage regulation of the subsequently iteration until the algorithm convergence. The flowchart of SMO based MPPT method is demonstrates in Fig. 2. The primary population of the duty cycle is to drive the boost converter. Afterwards, the PV current along with voltage corresponding to the duty cycle is measured. The evaluated values used for estimating the PV system power that represents the value of fitness. After the step of operation completed the maximum PV power is selected as the best and the corresponding d is saved as a best one.

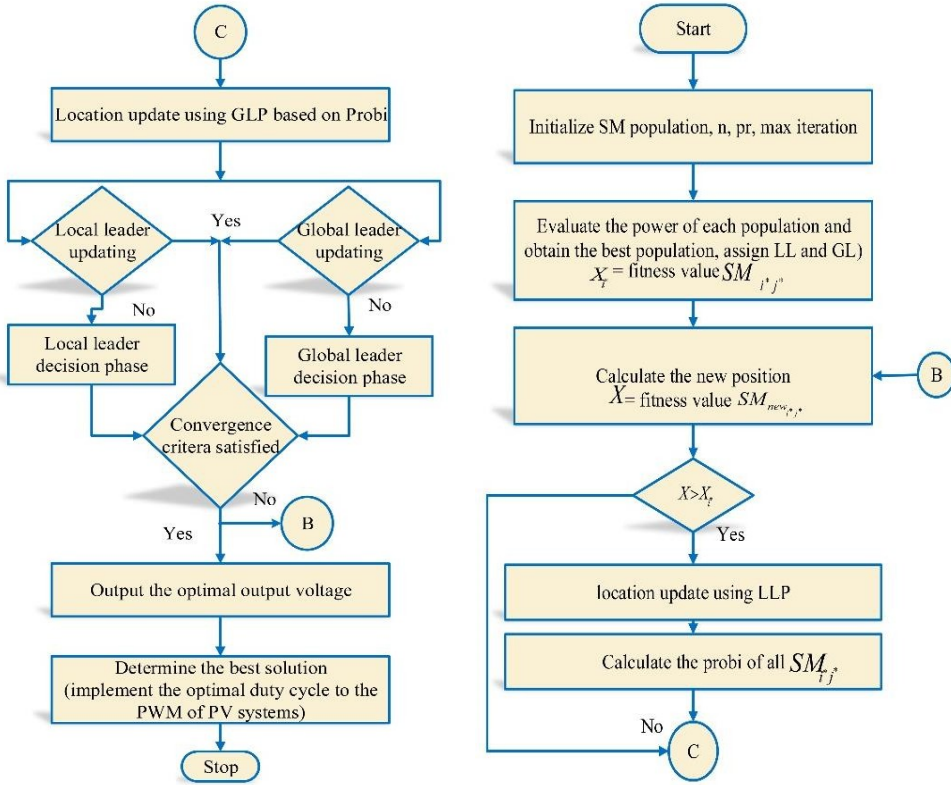


Figure 2: Flow Chart of SMO based MPPT algorithm

3.3. DC-DC boost converter

DC-DC converter is to attain the maximum power from the solar PV panel [21] and increase its output voltage. To accomplish these, the DC bus voltage (V'_{DC}) is sensed from the PV output voltage, current as well as the DC-DC boost converter output voltage. The control of the duty cycle d necessary is adjusted for controlling the IGBT of the converter. The PV array reference voltage V'_{rf} along with the V'_{DC} of VSC is utilized to evaluate the mention duty ratio for the boost converter. The inductor value is calculated by the Eq. (1) as

$$L_i = \frac{V'_{PV}d}{(2f_{st}\Delta i'_L)}, \quad (10)$$

where, the duty cycle (d) is estimated $d = 1 - \left(\frac{V'_{PV}}{V'_{out}}\right) = 0.13$, the converter boost the $V'_{PV} = 351$ to $V'_{DC} = 500$ V from the SMO based MPPT, $\Delta i'_L$ is the output ripple current and so as to meant for this converter develop the value of $\Delta i'_L$ is

taken as 10% of the input current $i'_L = (P'_{PV}/V'_{PV})$ which is achieved around 31 A, the calculated value of $\Delta i'_L$ is 3.1 A and switching frequency f_{st} at 10 kHz. The selected inductor value is 5 mH for the purpose of simulation.

3.4. DC-link capacitor

The DC link capacitor coupled to VSC is designed based on the transient time which is calculated by the Eq. (11) as

$$C'_{DC} = \frac{P'_{DC}/V'_{DC}}{2 * w * V'_{DCrip}} = \frac{11000/500}{2 * 3.14 * 0.02 * 500} = 3203.18 \mu\text{F}, \quad (11)$$

where, the percentage of ripple voltage V'_{DCrip} taken as the DC connection voltage is 2% and the angular frequency is assigned as $w = 2\pi * 50$ rad/s. Hence, the DC link capacitor of 4000 μF is selected. From this the disturbances in the DC connection voltage can be maintained.

3.5. AC inductor design

The design of AC inductor in inverter based on Δ_i , f_{st} is denoted as switching frequency, V'_{DC} and L'_f is evaluated by the Eq. (12) as,

$$L'_f = \frac{\sqrt{3}m_i V'_{DC}}{120_f f_{st} \Delta_i}, \quad (12)$$

where, the modulation index is represented in m_i , the overload factor is $O_f = 1.2$, $\Delta_i = 5\%$, $f_{st} = 10$ kHz, $V'_{DC} = 500$ V and the L'_f value is obtained to be 5 mH.

3.6. Lattice Levenberg–Marquardt recursive least squares control design

In this paper, the control design includes the proposed VSC switching pulse generation of the LLMRLS control algorithm. The switching algorithm of converters proposes the estimation of the elementary weight extraction, terminal voltage, active and reactive loss of elements, the feed forward elements of SPV and 3φ reference currents of the grid. The VSC in the grid injected a reference current, which is controlled by the hysteresis current controller. The proposed control algorithm is displayed in Fig. 3. The Conventional filter is correlated to the LLMRLS but it needs to associates with lesser arithmetic operation. The advantages of this proposed control algorithm over the conventional algorithms are modular structure, faster convergence rates and the key link matrix of Eigen value differences.

• The weight extraction of elementary active and reactive power

The LLMRLS algorithm explains the posteriori error and comprises into the stabilized form. In the forward forecast form $r(k') = y(k')$ with most of the test in-

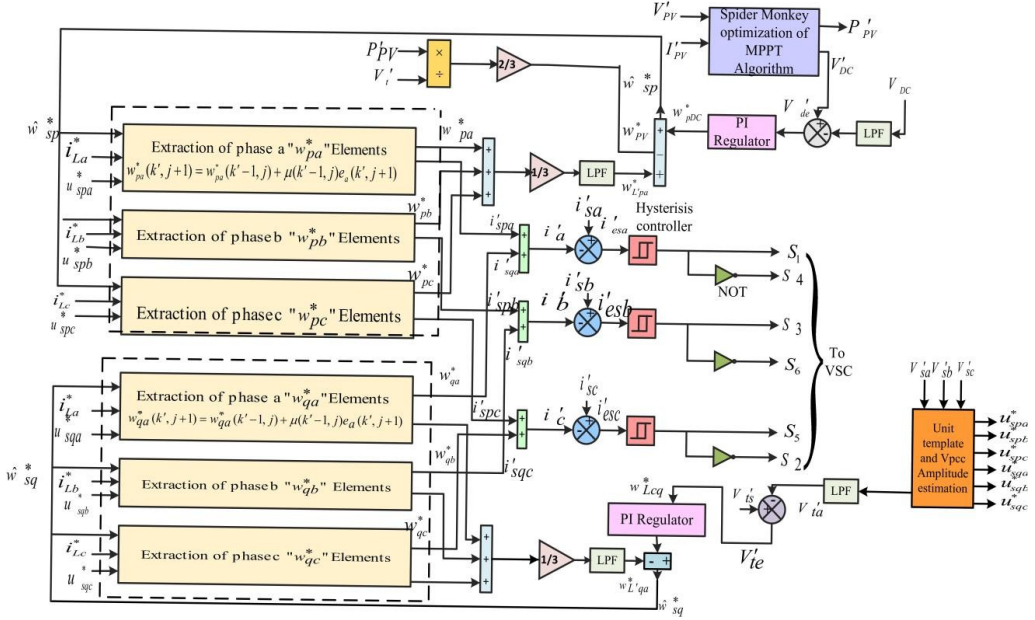


Figure 3: Proposed control algorithm

put signal is $y(k'-1)$. The backward forecast form $r(k') = y(k'-j-1)$, where j is the past test index for the forecast errors and $y(k')$ is the key signal of the most related analysis. The input vectors are $y(k') = [y(k'), y(k'-1), \dots, y(k'-j-1)]$. The forward and backward forecast of posteriori error is computed using Eq. (13) and Eq. (14) for the weight vector as

$$\varepsilon'_f(k', j+1) = r(k') - w_f^T(k', j) y(k'-1, j), \quad (13)$$

$$\varepsilon'_b(k', j+1) = r(k') - w_b^T(k', j) y(k'-1, j). \quad (14)$$

The forward and backward forecast of priori errors are estimated using Eq. (15) and Eq. (16) by the drain weight vector of the previous predictor,

$$e'_f(k', j+1) = r(k') - w_f^T(k'-1, j) y(k'-1, j), \quad (15)$$

$$\varepsilon'_b(k', j+1) = e_b(k', j) \delta(k'j). \quad (16)$$

The weights extraction of the forward and backward vector in Eq. (17) and Eq. (18) is evaluated as,

$$w_f(k', j+1) = w_f(k'-1, j) + \mu(k'-1, j) e_f(k'j+1), \quad (17)$$

$$w_b(k', j+1) = w_b(k'-1, j) + \hat{\mu}(k'-1, j) + \hat{\mu}(k', j) \varepsilon'_b(k'j+1), \quad (18)$$

where, $w^T(k')y(k')$ is calculated as the output for the known input $y(k')$ and $w(k')$ is the weight value, $w_{k'f}^T$ and $w_{k'b}^T$ are row vectors, $\epsilon'_f(k'j + 1)$ is the forward forecast posteriori error at time k' , $\epsilon'_b(k'j + 1)$ is the backward forecast posteriori error at time k' , $e_f(k'j + 1)$ is the forward forecast priori error, $e_b(k', j)$ is the backward forecast priori error, $\delta(k'j)$ is the conversion factor, w_f and w_b is the forward and backward weight estimation, μ and $\hat{\mu}$ are the gain vectors. The time-update Eqs. (19) and (20) of the least square (LS) sum of the forward as well as backward forecast errors at time k' are calculated as,

$$\xi_{f \min}^r(k', j + 1) = \lambda \xi_{f \min}^r(k' - 1, j) + e_f(k', j) \epsilon'_f(k'j), \quad (19)$$

$$\xi_{b \min}^r(k', j + 1) = \lambda \xi_{b \min}^r(k' - 1, j) + e_b(k', j) \epsilon'_b(k'j), \quad (20)$$

where the minimum LS backward forecast error is denoted $\xi_{c \min}^e(k', j)$ and forward error forecast is denoted as $\xi_{g \min}^e(k', j)$. In Lattice RLS, the Levenberg-Marquard algorithm is added which is used to solve the non-linear LS problem in the control algorithm. Simply if the previous estimation is close to the final estimation, then only the algorithm yields to the overall minimum value. The parameter vectors $\xi_{f/b \min}^r$ is denoted a new estimate of $\xi_{f/b \min}^r + \delta$. To determine δ , the function $g(y_j, \xi_{f/b \min}^r + \delta)$ is approximated by its linearization in Eq. (21) follows as,

$$g(y_j, \xi_{f/b \min}^r + \delta) \approx g(y_j, \xi_{f/b \min}^r) + w^T \gamma, \quad (21)$$

where, w^T is the row vector of g with respect to $\xi_{f/b \min}^r$. The sum of $T(\xi_{f/b \min}^r)$ is denoted as the square deviation its minimum at a zero ascent with respect to $\xi_{f/b \min}^r$ and the above first order estimate is given in Eq. (22) as,

$$T(\xi_{f/b \min}^r + \gamma) \approx \sum_{j=1}^n [z_j - g(y_j, \gamma) - w_j^T \gamma]^2, \quad (22)$$

where w is the Jacobian matrix, j -th is the row vector of w_j which can be solved by the linear calculation for γ . Moreover, based on the Lattice order the updated forward as well as backward extracted weights are uniform and normally it is denoted as $w^*(k', j + 1)$. Furthermore, the elementary active power elements are extracted which are rewritten for three phases in Eqs. (23), (24) and (25) as follows

$$w_{pa}^*(k', j + 1) = w_{pa}^*(k' - 1, j) + \mu(k' - 1, j) e_a(k'j + 1), \quad (23)$$

$$w_{pb}^*(k', j + 1) = w_{pb}^*(k' - 1, j) + \mu(k' - 1, j) e_b(k'j + 1), \quad (24)$$

$$w_{pc}^*(k', j + 1) = w_{pc}^*(k' - 1, j) + \mu(k' - 1, j) e_c(k'j + 1). \quad (25)$$

Similarly, the elementary reactive power elements are extracted which are for three phase Eqs. (26), (27) and (28) as follows

$$w_{qa}^* (k', j + 1) = w_{qa}^* (k' - 1, j) + \mu (k' - 1, j) e_a(k'j + 1), \quad (26)$$

$$w_{qb}^* (k', j + 1) = w_{qb}^* (k' - 1, j) + \mu (k' - 1, j) e_b(k'j + 1), \quad (27)$$

$$w_{qc}^* (k', j + 1) = w_{qc}^* (k' - 1, j) + \mu (k' - 1, j) e_c(k'j + 1), \quad (28)$$

where, w_{pa}^* , w_{pb}^* , w_{pc}^* are the extracted weight of elementary active power and w_{qa}^* , w_{qb}^* , w_{qc}^* is the extracted weights of the elementary reactive power.

• Terminal voltage estimation

The phase voltage v'_{sa} , v'_{sb} , v'_{sc} is calculated by sensed the line voltages. These voltages are passed via a low-pass filter to eliminate the distortion. The terminal voltage of amplitude is evaluated in Eq. (29) as

$$V'_{ta} = \sqrt{\frac{2}{3}} (v'^2_{sa} + v'^2_{sb} + v'^2_{sc}). \quad (29)$$

The in-phase models are estimated by dividing the phase voltages by amplitude of terminal voltages respectively in Eq. (30) as follows

$$u^*_{spa} = \frac{V'_{sa}}{V'_{ta}}, \quad u^*_{spb} = \frac{V'_{sb}}{V'_{ta}}, \quad u^*_{spc} = \frac{V'_{sc}}{V'_{ta}}. \quad (30)$$

In the VSC control the input vectors of in-phase for the reference active grid current generation is represented as $(u^*_{spa}, u^*_{spb}, u^*_{spc})$.

• Evaluation of active and reactive loss of elements

After the calculation of V'_{ta} , the error voltage $V'_{te}(k')$ of the voltage at the PCC and the reference value of terminal voltage ($V'_{ts} = 340$ V peak of the amplitude of phase V) is fed to a PI controller. The error at the k' sampled time in Eq. (31) is given as

$$V'_{te}(k') = V'_{ts}(k') - V'_{ta}(k'). \quad (31)$$

The output of PI voltage controller in the reactive loss component w^*_{Lcq} which is used to maintain the voltage at the PCC in Eq. (32) as,

$$w^*_{Lcq}(k' + 1) = w^*_{Lcq}(k') + \hat{K}_{pt} (V'_{te}(k' + 1) - V'_{te}(k')) + \hat{K}_{lt} V'_{te}(k' + 1), \quad (32)$$

where \hat{K}_{pt} and \hat{K}_{lt} are the integral and proportional constants used in PI voltage controller. Similarly, the voltage is sensed at V_{DC} of VSC and compared with reference DC bus voltage V'_{DC} achieved from the maximum power point tracking.

The error V'_{De} is generated and forwarded across the PI controller. The error at the k' sampled time in Eq. (33) is given as,

$$V'_{De}(k') = V'_{DC}(k') - V'_{DC}(k'). \quad (33)$$

The outcome of PI voltage controller in the active loss component w^*_{pDC} , which is used to normalize the DC link voltage, is computed using Eq. (34) as follows,

$$w^*_{Lcp}(k' + 1) = w^*_{Lcp}(k') + \hat{K}_{pD} (V'_{te}(k' + 1) - V'_{De}(k')) \\ + \hat{K}_{ID} V'_{De}(k' + 1), \quad (34)$$

Where, \hat{K}_{ID} is the integral and \hat{K}_{pD} is the proportional constants employs in PI voltage controller of active loss elements.

• **Feed forward SPV estimation**

The three phases are computed from Solar PV power and magnitude of PCC voltage in Eq. (35) as follows,

$$w^*_{PV} = \frac{2P'_{PV}}{3V'_t}, \quad (35)$$

where the rest of the Solar PV power is P'_{PV} and V'_t is the magnitude of PCC voltage.

• **The three phase grid reference current generation**

The reference current production in three phase *grid* the total weight of elements active power \hat{w}^*_{sp} is calculated in Eq. (36) by summing the DC loss element to average elementary active weight element and the feed-forward Solar PV weight is calculated.

$$\hat{w}^*_{sp} = w^*_{L'pa} + w^*_{Lcq} - w^*_{PV}, \quad (36)$$

where the average weights $w^*_{L'pa}$ equivalent to elementary active w^*_{pa} , w^*_{pb} , w^*_{pc} power elements are computed as $w^*_{L'pa} = (w^*_{pa} + w^*_{pb} + w^*_{pc}) / 3$.

The active reference elements of grid currents are expressed by the Eq. (37) as follows

$$i'_{spa} = \hat{w}^*_{sp} \cdot u^*_{spa}, \quad i'_{spb} = \hat{w}^*_{sp} \cdot u^*_{spb}, \quad i'_{spc} = \hat{w}^*_{sp} \cdot u^*_{spc}. \quad (37)$$

Thus, the total reactive weight elements of the reference grid currents are calculated by taking the average elementary reactive weight elements to the AC loss component in Eq. (38) as follows,

$$\hat{w}^*_{sq} = w^*_{Lcq} - w^*_{L'qa}. \quad (38)$$

Reference grid current elements are expressed in Eq. (39) as follows,

$$i'_{sqa} = i'_{qa}, \quad i'_{sqb} = i'_{qb}, \quad i'_{sqc} = i'_{qc}. \quad (39)$$

The addition of active power elements current and the reactive power elements current is known as a total reference grid current

• **Generation of gating signals**

To generate the signals of gating for IGBTs switching's of the VSC, a PWM current controller technique such as Hysteresis Current controller is used. (i'_a, i'_b, i'_c) are the reference current, which, are compared with the $(i'_{sa}, i'_{sb}, i'_{sc})$ of sensed current in the gate pulse current controller. Consequently, the current errors are amplified, and the output of the amplified current is contrasted with the switching frequency to signals of gating generation for the switching of Inverter. The HC controller is employed for controlling VSC to force the grid current such that it follows the reference current

4. Simulation results and discussion

The proposed double-stage three phase of PV power system is modeled and simulated in MATLAB/Simulink. The performance of the grid integrated PV system is displayed in Figs. 4 to 8. The proposed SMO algorithm extracts the maximum power from PV array an effectively and the LLMRLS based control for enhanced the behavior under balanced, unbalanced nonlinear loads and during the sudden variation of Solar Insolation.

4.1. Performance of the proposed SPV system under balanced nonlinear load

The performance of the PV system under balanced nonlinear load is shown in Fig. 4. A nonlinear load of 11 kW and lagging power factor of 0.8 is connected to the PV system. The behavior of the system is shown for 0.1 to 0.8 s. At instance $t = 0.1$ s the structure is functioning in PF correction approach. The Solar PV power is more than the 11 kW, so the power sustained to the grid is divergence, which is examined in the Fig. 4b. The balancing nonlinear loads in the grid, turns the grid current is balanced at the unity PF.

4.2. Performance of the proposed SPV system under unbalanced nonlinear load

The behavior of the PV system under unbalanced nonlinear load state is shown in Fig.5. A load of 11 kW is connected to the PV system and the performance of the PV system is examined. As a result, the load currents are close to be sinusoidal despite there is an unbalanced load, but the grid currents are sinusoidal. At time $t = 0.1$ s, the nonlinear loads are disconnected phase a, due to which load turn

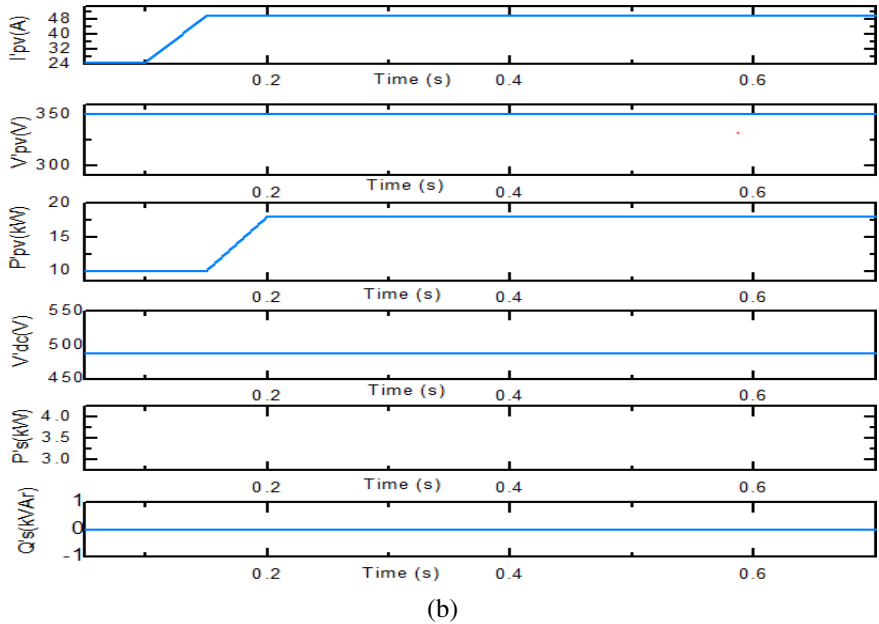
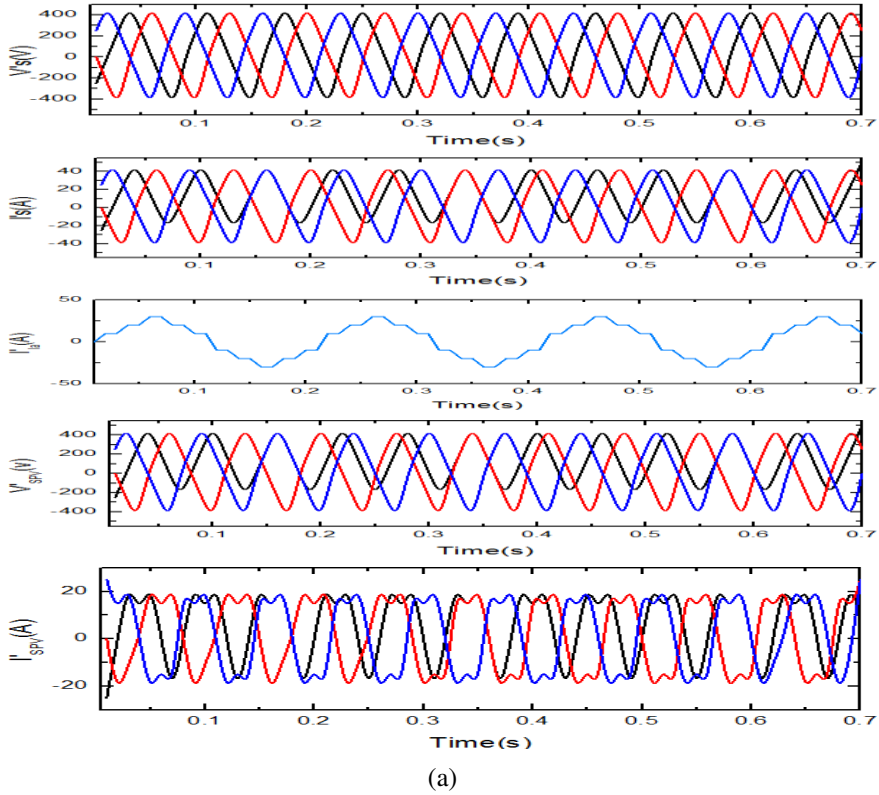
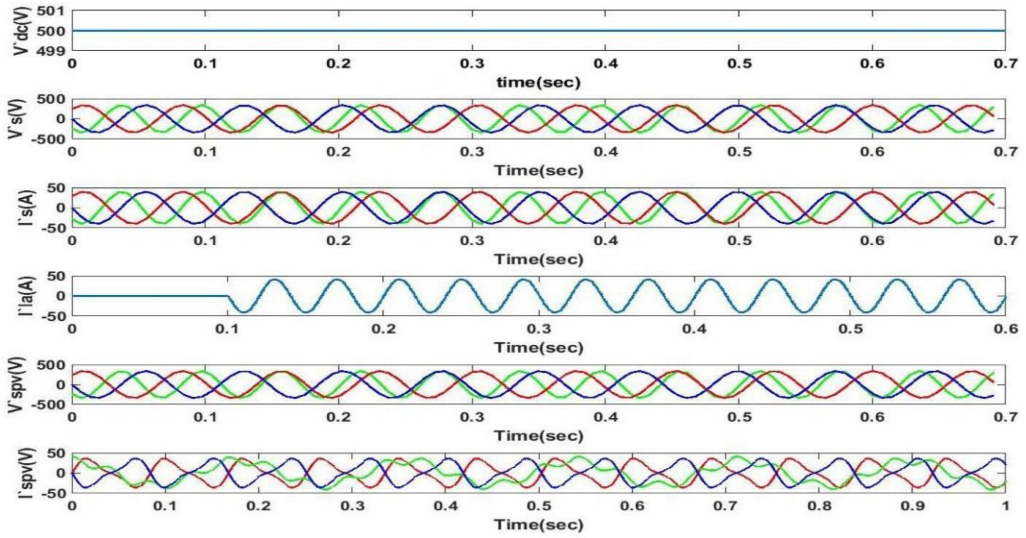
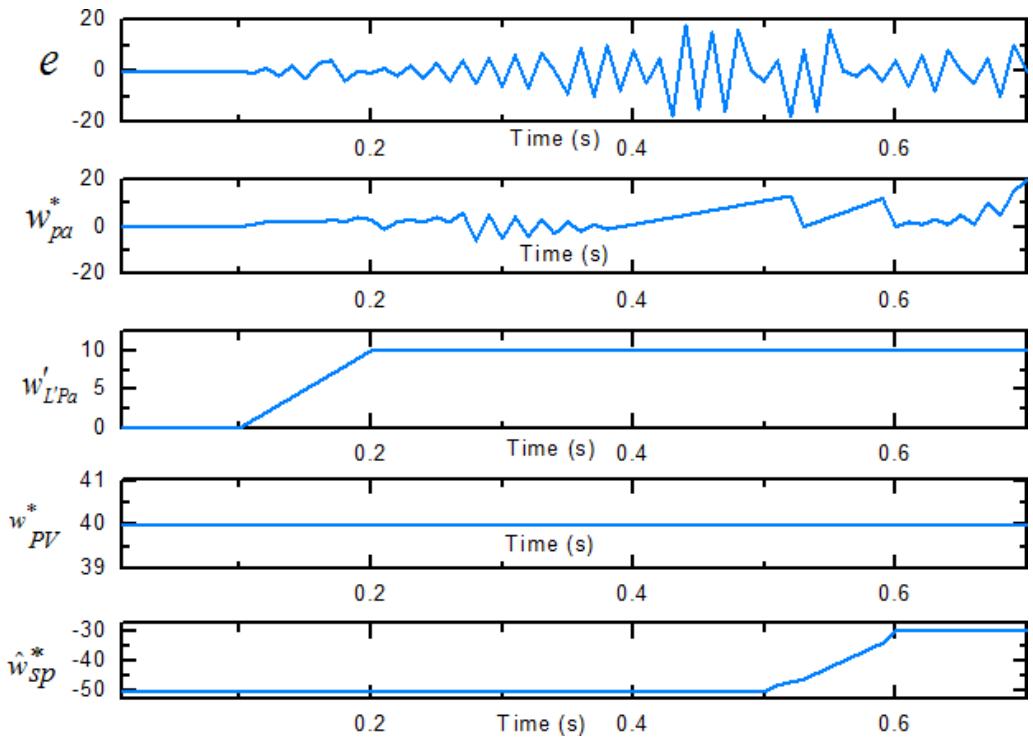


Figure 4: Behavior of the proposed PV system under balanced nonlinear loads



(a)

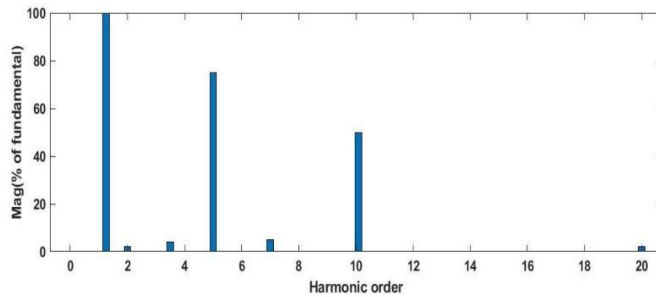


(b)

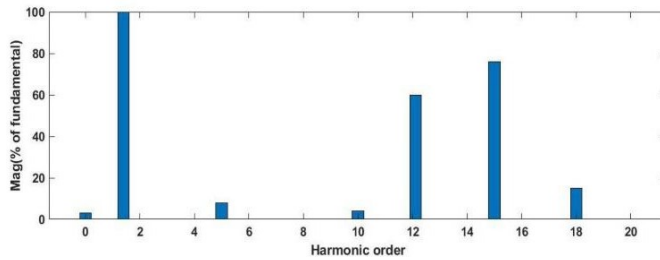
Figure 5: Behavior of the proposed PV system under unbalanced nonlinear loads

out to be unbalanced even though the currents of grid are sinusoidal in addition to balanced. Moreover, due to the load power reduction the grid current is examined. The unbalanced and non-sinusoidal currents of VSC to create the balanced and sinusoidal grid currents, which is gratify the THDs of voltage of PCC, grid current and load currents within the IEEE standards. The gate signal of the reference current is regulated by the HC controller, where the value $\delta = 0.019$.

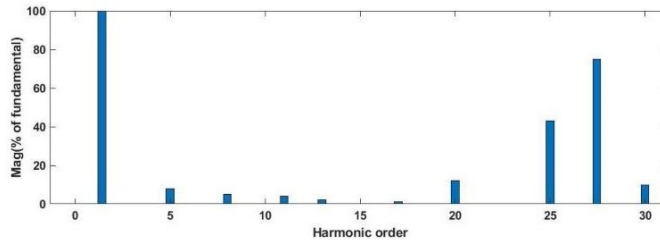
The THD in grid coordinated system voltage of the PCC, grid current and load current under without compensation state is shown in Fig. 6. Under, the active power filter is removed at a certain time delay the THD obtained from the conditions in terms of PCC voltage is 10.50% at 238 V, Grid current is 12.30% at 26.28 A and the Load current is 27.80% at 25.53 A, respectively. However,



(a)



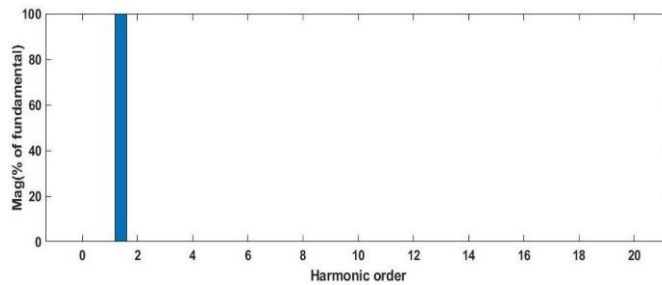
(b)



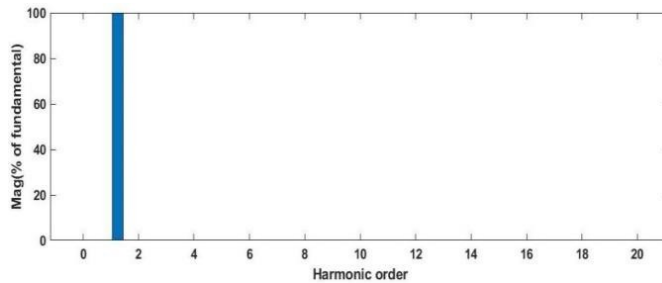
(c)

Figure 6: Harmonic spectra of PCC voltage, grid current and load current without compensation

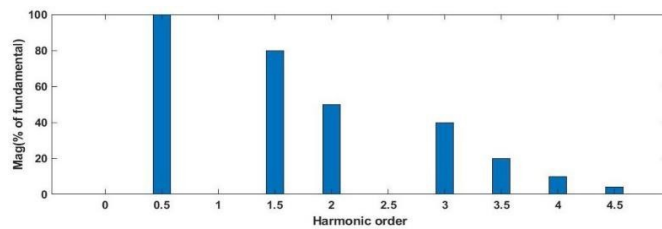
when the active filter of proposed controller is added to the coupled system then the THD value of PCC voltage is 1.25% at 240 V, Grid current is 1.75% at 17.23 A and the Load current is 4.43% at 18.64 A are obtained. The THD value of PCC voltage, grid current and Load current under with compensation state is shown in Fig. 7.



(a)



(b)



(c)

Figure 7: Harmonic spectra of PCC voltage, grid current and load current with compensation

4.3. Performance of the proposed solar PV system for immediate increase in step insolation of solar

The performance of the control scheme with step variation of solar irradiance is shown in Fig. 8. The solar irradiance varied from 500 W/m^2 to 1000 W/m^2 . The power from the PV is not sufficient to fulfill the demand of the load power ahead

of $t = 0.1$ s, therefore $-ve$ power flow to the load. Similarly, the Solar insolation is changed at the time $t = 0.1$ s, consequently the power is immediately increased due to the immediate PV current rises and afterwards the tracked the MPP. The power flow track is changed subsequently to the time $t=0.1$ s and separated among the load and the grid by the power as of the SPV array. Furthermore, in the transformation system of SPV energy the additional power is sustained to the grid at PF is unity.

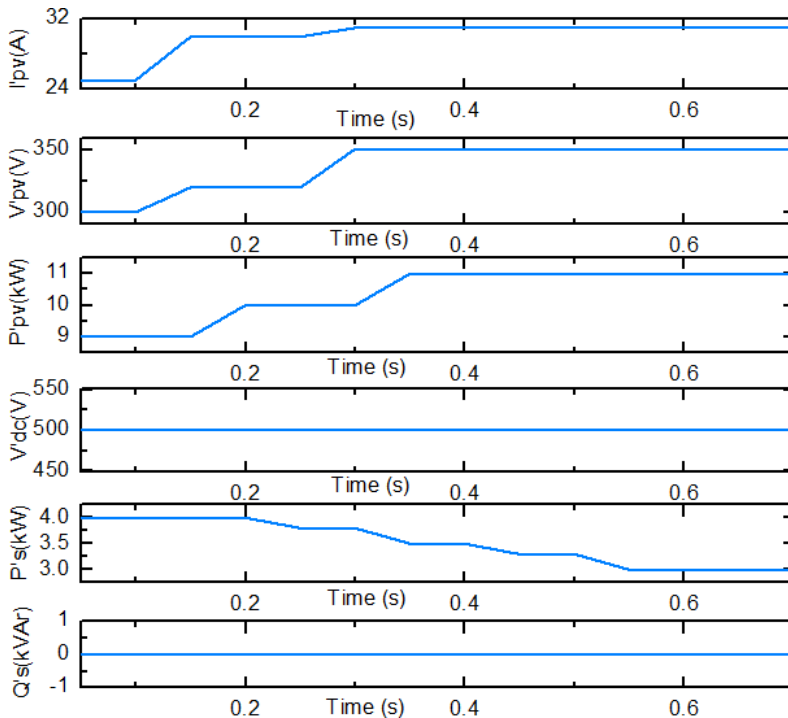


Figure 8: Behavior of the system at the increase in step of solar insolation

At the time of high penetration of PV from 500 W/m^2 to 1000 W/m^2 also, the real power P 's (kW) is regulated as 3kW and the reactive power Q 's (kW) is maintained as zero. Thus, the control method has been regulated the power system network by reducing the reactive power in the grid. Consequently, the phase and frequency problems are resolved by this projected method. Hence, the stability of dc voltage is maintained constant.

4.4. Comparative behavior with LLMRLS controller with conventional controllers

The LLMRLS based controller is compared with Zero Attracting-least Mean Square (ZA-LMS) [22], Lyapunov function with sliding mode controller (SMC) [23], and Maximize-M Kalman filter (MMKF) [24]. The ZA-LMS convergence

is slow compared to the proposed control technique. Furthermore, the major limitation of this method of SMC controller is chattering occurrence, as because of control signal can persuades various unwanted oscillations. At some stages the gain controller system parameters are not measured properly, this leads suffer in transition periods. Sequentially the MMKF has some limitation due to its complex structure. The proposed controller diminishes the limitations of the existing controllers, moreover the balanced and the unbalanced nonlinear load states of the load current weighted value meeting is shown.

The elementary weight of load current depends upon the load moreover the solar irradiance of both bus PI controller's outcomes. At instant $t = 0.1$ s the loads are unbalanced and after that the loads are coupled in the system. The proposed controller average active weight extraction is less compared to the other controllers also, it is enhanced response in the balanced and unbalanced state and fast convergence is obtained. The conventional controllers are slow convergence and high oscillation. The proposed controller functions are contrasted with the other controllers, which are revealed in Table 1.

Table 1: Comparison of proposed controller over conventional controllers

Contro Algorithm /Function		Proposed LLMRLS	ZA-LMS	Lyapunov function-SMC	MMKF
Computational complexity		Low	High	High	High
Nonlinear controller		HC	PI	SMC	HC
Error stability		Low	High	High	High
Weights convergence	Balanced	Fast	Slow	Slow	Slow
	Unbalanced	Fast	Slow	Slow	Slow
THD	Grid current	17.23 A, 1.75%	18.64 A, 1.95%	18.23 A, 4.07%	18.73 A, 1.95%
	Load current	18.64 A, 4.43%	20.57 A, 26.56%	18.75 A, 19.44%	18.45 A, 13.47%
Sample time (t_s)		10 μ s	50 μ s	75 μ s	300 μ s

The THD obtained from the projected method under the drastic conditions of grid current is 1.75% and load current is 4.43%, which is significantly limited within the standard of IEEE over the conventional methods. Consequently, the sample time of the proposed system is 10 μ s that is less while contrasted with the old techniques used in control process of grid coordinated system. Moreover, the proposed SMO based MPPT is compared with the conventional Backtracking Search Optimization (BSO) [29] and Artificial Bee Colony Integrated Perturb & Observe (ABC-PO) [30] methods, which is demonstrated in Table 2.

Table 2: Comparison of proposed SMO based MPPT over conventional optimization methods

MPPT Methods	Achieved output power	Accuracy	Tracking speed(s)	Efficiency (%)
BSO	113.67 W	Small	1.2	90%
ABC-PO	45 W	High	0.08	99.93
Proposed SMO	11 kW	Extremely high	0.04	99.96

Compare to the conventional MPPT methods, the projected SMO has obtained finest tracking in terms of tracking speed, efficiency, accuracy and achieved output power. Thus, the overall comparison of the developed system proved the significant improvement of grid coordinated development using the projected technique.

5. Conclusion

A grid connected solar PV has been formulated and the behavior of the grid should be enhancing by a novel control algorithm. In this paper, the SPV array has been coupled to the grid with three phase VSC, which has been self-sustained DC bus and infusing inductors. Moreover, the control algorithm based on LLMRLS method has been advanced for control of reference grid currents generation and gating pulses for the 3ϕ VSC. Consequently, the behavior of the advanced control design has demonstrated and the satisfactory operation of load power demand is attained along with the power quality issues such as the UPF maintaining, harmonic removal and load unbalancing. Grid current is achieved at 1.75% of THD in the PF correction and the PCC voltage along with the Load current THDs also satisfied within the limit of IEEE 519 standard. The efficient and consistent performances of SMO based MPPT algorithm, LLMRLS based control algorithm obtained in the balanced state, and unbalanced states of the grid interfaced SPV systems.

References

- [1] I. DINCER: Renewable energy and sustainable development: a crucial review. *Renewable and Sustainable Energy Reviews*, 4(2), (2000), 157–175, DOI: [10.1016/S1364-0321\(99\)00011-8](https://doi.org/10.1016/S1364-0321(99)00011-8).
- [2] S. GULKOWSKI, J.V.M. DIEZ, J.A. TEJERO, and G. NOFUENTES: Computational modeling and experimental analysis of heterojunction with intrinsic

- thin-layer photovoltaic module under different environmental conditions. *Energy*, **172**, (2019), 380–390, DOI: [10.1016/j.energy.2019.01.107](https://doi.org/10.1016/j.energy.2019.01.107).
- [3] M. BAHRAMI, et al.: Hybrid maximum power point tracking algorithm with improved dynamic performance. *Renewable Energy*, **130**, (2019), 982–991, DOI: [10.1016/j.renene.2018.07.020](https://doi.org/10.1016/j.renene.2018.07.020).
- [4] K.V. SINGH, KRISHNA, H. BANSAL, and D. SINGH: A comprehensive review on hybrid electric vehicles: architectures and components. *Journal of Modern Transportation*, **27**, (2019), 1–31, DOI: [10.1007/s40534-019-0184-3](https://doi.org/10.1007/s40534-019-0184-3).
- [5] S. PRADHAN, et al.: Performance Improvement of Grid-Integrated Solar PV System Using DNLMs Control Algorithm. *IEEE Transactions on Industry Applications*, **55**(1), (2019), 78–91, DOI: [10.1109/TIA.2018.2863652](https://doi.org/10.1109/TIA.2018.2863652).
- [6] S. NEGARI and D. XU: Utilizing a Lagrangian approach to compute maximum fault current in hybrid AC–DC distribution grids with MMC interface. *High Voltage*, **4**(1), (2019), 18–27, DOI: [10.1049/hve.2018.5087](https://doi.org/10.1049/hve.2018.5087).
- [7] V.T. TRAN et al.: Mitigation of Solar PV Intermittency Using Ramp-Rate Control of Energy Buffer Unit. *IEEE Transactions on Energy Conversion*, **34**(1), (2019), 435–445, DOI: [10.1109/TEC.2018.2875701](https://doi.org/10.1109/TEC.2018.2875701).
- [8] A. KIHAL, et al.: An improved MPPT scheme employing adaptive integral derivative sliding mode control for photovoltaic systems under fast irradiation changes. *ISA Transactions*, **87**, (2019), 297–306, DOI: [10.1016/j.isatra.2018.11.020](https://doi.org/10.1016/j.isatra.2018.11.020).
- [9] A.M. JADHAV, N.R. PATNE, and J.M. GUERRERO: A novel approach to neighborhood fair energy trading in a distribution network of multiple microgrid clusters. *IEEE Transactions on Industrial Electronics*, **66**(2), (2019), 1520–1531, DOI: [10.1109/TIE.2018.2815945](https://doi.org/10.1109/TIE.2018.2815945).
- [10] A. FRAGAKI, T. MARKVART, and G. LASKOS: All UK electricity supplied by wind and photovoltaics – The 30–30 rule. *Energy*, **169**, (2019), 228–237, DOI: [10.1016/j.energy.2018.11.151](https://doi.org/10.1016/j.energy.2018.11.151).
- [11] S.Z. AHMED, et al.: Power quality enhancement by using D-FACTS systems applied to distributed generation. *International Journal of Power Electronics and Drive Systems*, **10**(1), (2019), 330, DOI: [10.11591/ijpeds.v10.i1.pp330-341](https://doi.org/10.11591/ijpeds.v10.i1.pp330-341).
- [12] H.H. ALHELOU, et al.: A Survey on Power System Blackout and Cascading Events: Research Motivations and Challenges. *Energies*. **12**(4), (2019), 1–28, DOI: [10.3390/en12040682](https://doi.org/10.3390/en12040682).
- [13] M. BADONI, A. SINGH, and B. SINGH: Implementation of Immune Feedback Control Algorithm for Distribution Static Compensator. *IEEE*

- Transactions on Industry Applications*, **55**(1), (2019), 918–927, DOI: [10.1109/TIA.2018.2867328](https://doi.org/10.1109/TIA.2018.2867328).
- [14] S.R. DAS, et al.: Performance evaluation of multilevel inverter based hybrid active filter using soft computing techniques. *Evolutionary Intelligence* (2019), 1–11, DOI: [10.1007/s12065-019-00217-6](https://doi.org/10.1007/s12065-019-00217-6).
- [15] F. CHISHTI, S. MURSHID, and B. SINGH: LMMN Based Adaptive Control for Power Quality Improvement of Grid Intertie Wind-PV System. *IEEE Transactions on Industrial Informatics*, **15**(9), (2019), 4900–4912, DOI: [10.1109/TII.2019.2897165](https://doi.org/10.1109/TII.2019.2897165).
- [16] S. PRADHAN, et al.: Performance Improvement of Grid-Integrated Solar PV System Using DNLMs Control Algorithm. *IEEE Transactions on Industry Applications*, **55**(1), (2019), 78–91, DOI: [10.1109/IICPE.2016.8079455](https://doi.org/10.1109/IICPE.2016.8079455).
- [17] V. JAIN, I. HUSSAIN, and B. SINGH: A HTF-Based Higher-Order Adaptive Control of Single-Stage Grid-Interfaced PV System. *IEEE Transactions on Industry Applications*, **55**(2), (2019), 1873–1881, DOI: [10.1109/TIA.2018.2878186](https://doi.org/10.1109/TIA.2018.2878186).
- [18] N. KUMAR, B. SINGH, B. KETAN PANIGRAHI and L. XU: Leaky Least Logarithmic Absolute Difference Based Control Algorithm and Learning Based InC MPPT Technique for Grid Integrated PV System. *IEEE Transactions on Industrial Electronics*. **66**(11), (2019), 9003–9012, DOI: [10.1109/TIE.2018.2890497](https://doi.org/10.1109/TIE.2018.2890497).
- [19] P. SHAH, I. HUSSAIN, and B. SINGH: Single-Stage SECS Interfaced with Grid Using ISOGI-FLL- Based Control Algorithm. *IEEE Transactions on Industry Applications*, **55**(1), (2019), 701–711, DOI: [10.1109/TIA.2018.2869880](https://doi.org/10.1109/TIA.2018.2869880).
- [20] V. JAIN and B. SINGH: A Multiple Improved Notch Filter-Based Control for a Single-Stage PV System Tied to a Weak Grid. *IEEE Transactions on Sustainable Energy*, **10**(1), (2019), 238–247, DOI: [10.1109/TSTE.2018.2831704](https://doi.org/10.1109/TSTE.2018.2831704).
- [21] N. MOHAN and T. M. UNDELAND: *Power electronics: converters, applications, and design*. John Wiley & Sons, 2007.
- [22] M. BADONI, et al.: Grid interfaced solar photovoltaic system using ZA-LMS based control algorithm. *Electric Power Systems Research*, **160**, (2018), 261–272, DOI: [10.1016/j.epsr.2018.03.001](https://doi.org/10.1016/j.epsr.2018.03.001).
- [23] M. REZKALLAH, et al.: Lyapunov function and sliding mode control approach for the solar-PV grid interface system. *IEEE Transactions on Industrial Electronics*, **64**(1), (2016), 785–795, DOI: [10.1109/tie.2016.2607162](https://doi.org/10.1109/tie.2016.2607162).

- [24] N. KUMAR, B. SINGH, and B.K. PANIGRAHI: Integration of Solar PV with Low- Voltage Weak Grid System: using Maximize-M Kalman Filter and Self-Tuned P&O Algorithm. *IEEE Transactions on Industrial Electronics*, **66**(11), (2019), 9013–9022, DOI: [10.1109/tie.2018.2889617](https://doi.org/10.1109/tie.2018.2889617).
- [25] H. SHARMA, G. HAZRATI, and J.CH. BANSAL: *Spider monkey optimization algorithm*. *Evolutionary and swarm intelligence algorithms*. Springer, Cham, 2019, 43–59.
- [26] K. NEELU, P. DEVAN, CH.L. CHOWDHARY, S. BHATTACHARYA, G. SINGH, S. SINGH, and B. YOON: Smo-dnn: Spider monkey optimization and deep neural network hybrid classifier model for intrusion detection. *Electronics*, **9**(4), (2020), 692, DOI: [10.3390/electronics9040692](https://doi.org/10.3390/electronics9040692).
- [27] M.A.H. AKHAND, S.I. AYON, A.A. SHAHRIYAR, and N. SIDDIQUE: Discrete spider monkey optimization for travelling salesman problem. *Applied Soft Computing*, **86** (2020), DOI: [10.1016/j.asoc.2019.105887](https://doi.org/10.1016/j.asoc.2019.105887).
- [28] AVINASH SHARMA, AKSHAY SHARMA, B.K. PANIGRAHI, D. KIRAN, and R. KUMAR: Ageist spider monkey optimization algorithm. *Swarm and Evolutionary Computation*, **28** (2016), 58–77, DOI: [10.1016/j.swevo.2016.01.002](https://doi.org/10.1016/j.swevo.2016.01.002).
- [29] SRIRAM MOUNIKA and K. RAVINDRA: Backtracking Search Optimization Algorithm Based MPPT Technique for Solar PV System. In *Advances in Decision Sciences, Image Processing, Security and Computer Vision*. Springer, Cham, 2020, 498–506.
- [30] PILAKKAT, DEEPTHI and S. KANTHALAKSHMI: Single phase PV system operating under Partially Shaded Conditions with ABC-PO as MPPT algorithm for grid connected applications. *Energy Reports*, **6** (2020), 1910–1921, DOI: [10.1016/j.egy.2020.07.019](https://doi.org/10.1016/j.egy.2020.07.019).
- [31] R. GESSING: Controllers of the boost DC-DC converter accounting its minimum- and non-minimum-phase nature. *Archives of Control Sciences*, **19**(3), (2009), 245–259.
- [32] A. TALHA and H. BOUMAARAF: Evaluation of maximum power point tracking methods for photovoltaic systems. *Archives of Control Sciences*, **21**(2), (2011), 151–165.
- [33] S.N. SINGH and S. MISHRA: FPGA implementation of DPWM utility/DG interfaced solar (PV) power converter for green home power supply. *Archives of Control Sciences*, **21**(4), (2011), 461–469.